Annals of Biomedical Engineering, Vol. 36, No. 11, November 2008 (© 2008) pp. 1893–1908
DOI: 10.1007/s10439-008-9563-3

Non-Newtonian Bile Flow in Elastic Cystic Duct: One- and Three-Dimensional Modeling

W.G. Li,[1] X.Y. Luo,[1] S.B. Chin,[2] N.A. Hill,[1] A.G. Johnson,[3] and N.C. Bird[3]

[1]Department of Mathematics, University of Glasgow, Glasgow G12 8QW, UK; [2]Department of Mechanical Engineering, University of Sheffield, Sheffield S1 3JD, UK; and [3]Academic Surgical Unit, Royal Hallamshire Hospital, Sheffield S10 2JF, UK

(*Received 29 December 2007; accepted 4 September 2008; published online 13 September 2008*)

Abstract—Bile flow is thought to play an essential role in the pathophysiological genesis of cholelithiasis (gallstone formation) and in gallbladder pain. In this paper, we extend our previous study of the human biliary system (Li *et al*., 2007, *J. Biomech. Eng*., 129:164–173) to include two important factors: the non-Newtonian properties of bile, and elastic deformation of the cystic duct. A one-dimensional (1D) model is analyzed and compared with three-dimensional (3D) fluid–structure interaction simulations. It is found that non-Newtonian bile raises resistance to the flow of bile, which can be augmented significantly by the elastic deformation (collapse) of the cystic duct. We also show that the 1D model predicts the pressure drop of the cystic duct flow well for all cases considered (Newtonian or non-Newtonian flow, rigid or elastic ducts), when compared with the full 3D simulations.

Keywords—Gallbladder, Gallstone, Cystic duct, Biliary system, Non-Newtonian fluid, Pressure drop, Fluid–structure interaction, 1D modeling, Finite element methods.

NOMENCLATURE

Variables

A	Cross-sectional area of collapsed duct, m^2
A_{eq}	Cross-sectional area of duct at zero transmural pressure $A_{eq} = \pi d_{eq}^2/4$, m^2
A_1	Cross-sectional area of baffle clearance, m^2
c_2	Sudden expansion head-loss coefficient
c_4	Head-loss coefficient for a 90° bend
d	Internal diameter of duct, mm
E	Young's modulus of cystic duct wall, Pa
f	Darcy friction factor
f_0	Darcy friction factor for duct without baffles
h	Wall or baffle thickness, mm
H	Baffle height, mm
k, l	Exponent in tube laws
L	Length of duct, m
L_k	Extra length due to minor pressure losses, m
m	Power in the Carreau model
n	Number of baffles or exponent in tube law
n_c	Maximum number of baffles considered
p	Internal duct pressure, Pa
p_e	External duct pressure, Pa
Q	Bile flow rate, mL/min
Re	Reynolds number based on d_{eq} and μ_∞
u	Bile velocity in cystic duct, $u = Q/A$, m/s
V	Gallbladder volume, mL
x, y, z	Cartesian coordinates, m
α	Area ratio, $\alpha = A/A_{eq}$
γ	Shear rate, s^{-1}
λ	Time constant
ε	Velocity deformation rate or shear strain rate, s^{-1}
μ	Bile dynamic viscosity, Pa s
μ_0	Dynamic viscosity at zero shear rate, Pa s
μ_∞	Dynamic viscosity at infinite shear rate, Pa s
κ	Poisson's ratio of the cystic duct wall
ρ	Density of bile, kg/m^3
τ	Shear stress, Pa
ξ	Dimensionless baffle height, $\xi = H/d_{CD}$
Δp	Pressure drop, Pa
Δp_{te}	Minor pressure drop in T-junction during emptying, Pa
Δp_k	Pressure losses due to bends, sudden expansion and contraction, Pa

Subscripts

b	Baffle
CBD	Common bile duct
CD	Cystic duct
CHD	Common hepatic duct

Address correspondence to X.Y. Luo, Department of Mathematics, University of Glasgow, Glasgow G12 8QW, UK. Electronic mail: x.y.luo@maths.gla.ac.uk

EM	Emptying
eq	Equivalent
i	Coordinate index, $i = 1, 2, 3$
in	Inlet of duct
j	Coordinate index, $j = 1, 2, 3$
min	Minimum value
out	Outlet
RF	Refilling
w	On wall

INTRODUCTION

Cholelithiasis, also known as the presence of a gallstone, is one of the most common human biliary diseases. Clinical treatments for the diseases often involve the surgical removal of the gallbladder, known as cholecystectomy, which is the most often performed abdominal operation in the West.[8] Reduction in gallbladder motility leading to prolonged stasis of bile in the gallbladder is one of the essential factors in the pathogenesis of cholelithiasis.[10,26] Pitt *et al.*[38] showed experimentally that an increased resistance to flow (i.e. pressure drop) in the cystic duct, and not altered gallbladder compliance, is etiologically related to bile stasis. This suggests that a more detailed knowledge of fluid mechanics in the biliary system will contribute to understanding of the etiology of cholethiasis.

Motivated by this, a number of studies have been carried out on the fluid mechanics behavior of the biliary system. Ooi *et al.*[36] examined the effect of the cystic duct geometry on the flow resistance using both two (2D)- and three-dimensional (3D) cystic duct models. In their numerical study, the cystic duct was modeled as a straight pipe with two types of baffles, the numbers and heights of which were varied. The bile was assumed to be Newtonian, and its viscosity varied between 1 and 4 mPa s. The results were compared with more realistic 2D models based on patients' biliary system images. It was found that both the baffle height and number of baffles can significantly affect the flow resistance. In a further development, Li *et al.*[30] studied one-dimensional (1D) rigid and elastic wall models for the biliary system, including the cystic duct, and the T-junction of the common bile duct and hepatic duct. Cystic ducts with baffles were modeled using the concept of equivalent diameter and length, and were either rigid or elastic. However, in these studies, only Newtonian fluids were considered; the non-Newtonian rheology of the bile, the complicated geometry of cystic duct, and the soft tissue deformation and its interactions with the fluid were not fully taken into account.

Clinical measurements have demonstrated that the density of gallbladder bile is 965.9–1014.5 kg/m^3 [35] and its density is very close to that of water at 1000 kg/m^3 at 20 °C. However, the dynamic viscosity of gallbladder bile is found to be in the range of 1.77–8.0 mPa s,[35] which is very different to water. Some measurements of bile viscosity using a capillary tube viscometer[6,16] suggested that human bile behaves like a Newtonian fluid. However, Tera[42] and Thureron[44] found that the normal gallbladder bile is layered. For example, the dynamic viscosity of the top thinnest layer is 2.0 mPa s, but that of the thickest layer is 2.2 mPa s after 2 h of sedimentation.[42] The concentration of normal gallbladder bile is a major factor determining viscosity. In pathological and hepatic duct bile the content of mucous substances is the major factor determining viscosity. There is also evidence that the mean dynamic viscosity of bile in pathological gallbladders is greater than that of normal gallbladders and both are more viscous than that of hepatic duct bile.[6,16]

More recent measurements with concentric cylinder viscometers[13,21,35] showed that gallbladder bile behaves as a non-Newtonian fluid at low shear rates. Gottschalk and Lochner[21] measured the postoperative bile viscosity sampled by T-tube drainage in 29 patients with a modified horizontal capillary viscometer and discovered that the bile is shear thinning as well as viscoelastic. The shear-thinning characteristic of bile was also confirmed by Coene *et al.*,[13] and they found that the bile viscosity decreases from 2.5 mPa s at shear rate of 0.1 s^{-1} to 1.5 mPa s at 100 s^{-1}. Ooi[35] measured the bile dynamic viscosity of 59 patients (after cholecystectomy) and found that the bile rheology (the relation between stress and shear rate) was Newtonian for 20 patients, but either shear thinning or shear thickening for the rest of patients. These experiments suggest that gallbladder bile presents a complicated non-Newtonian behavior under different pathological conditions. In addition, the presence of mucus in gallbladders with stones also accounts for the differences in viscosity.[18] Jungst *et al.*[27] showed that the biliary viscosity is markedly higher in gallbladders with cholesterol (= 5.0 mPa s) and mixed stones (= 3.5 mPa s) compared to hepatic bile (= 0.2 mPa s). A positive correlation between mucin and viscosity was found in gallbladder bile but not in hepatic bile. Increased viscosity of gallbladder bile and its non-Newtonian behavior are thus considered to be important effects in the pathogenesis of gallstone disease.[27]

It has been shown that cholecystokinin (CCK) stimulation not only causes the gallbladder to contract, but also allows the cystic and common bile ducts to contract.[15,41] However, the sensitivity to CCK decreases from gallbladder to common bile duct.[30] This sensitivity gradient may act to facilitate gallbladder emptying in response to hormonal and neural

stimulation.[41] These facts suggest that the elastic deformation of the cystic duct is a contributing factor.

Three-dimensional fluid–structure interactions in smooth collapsible tubes have been examined extensively both experimentally,[3,4,7,14,24,25,28,32] and numerically.[22,23,33,40,43] However, it seems that very little attention has been paid to non-Newtonian flow in compliant ducts with staggered baffles.

In the present study, we focus on the characteristics of non-Newtonian bile flow and compare them with those of Newtonian bile. We extend our previous 1D model[30] to include the non-Newtonian effects of the gallbladder bile, as well as elastic deformation of the cystic duct. Given the relatively low Reynolds number for flows in this section, only steady flows are considered. The idealized cystic duct geometry of Ooi *et al.*[36] is adopted here, with the non-Newtonian fluid described by Carreau's equation.[47] The effects of cystic duct geometry, wall elasticity and rheological properties on pressure drop are examined in terms of the Darcy friction factor. In addition, 3D computational fluid dynamic and fluid–structure interaction simulations of Newtonian and non-Newtonian bile flows in an idealized cystic duct model of Ooi *et al.*[36] were also carried out to provide insights into the detailed flow structure and to validate and assess the new 1D model.

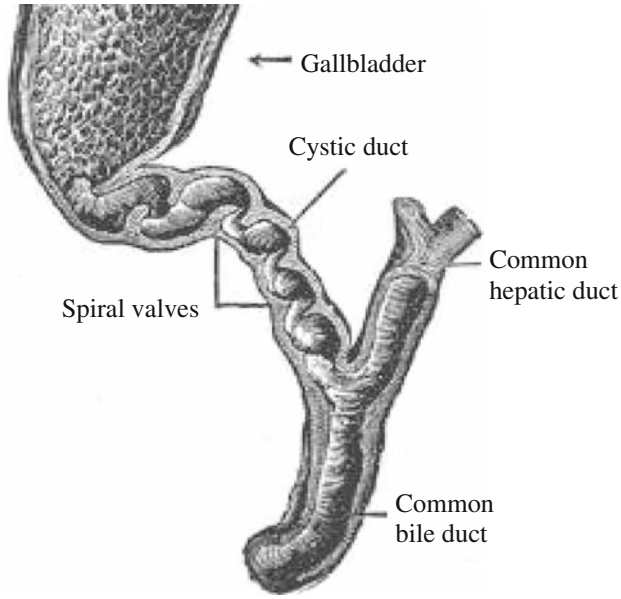

FIGURE 1. Gross anatomy of the human biliary tree showing part of the gallbladder neck connected to the spiral valves in the cystic duct (picture from http://www.en.wikipedia.org/).

THE 1D BILIARY SYSTEM MODEL

The Geometry

The human biliary system comprises the liver, gallbladder, and biliary tract (cystic, common hepatic, and common bile ducts), Fig. 1. The gallbladder is a thin-walled, pear-shaped sac which measures approximately 7–10 cm in length and 3 cm in width with an average storage capacity of 20–30 mL.[17] It connects to the cystic duct which is approximately 3.5 cm long and 3 mm wide and merges with the common bile duct. The mucosa of the cystic duct proximal to the gallbladder is arranged into 2–14 crescentic folds or valves known as the spiral valves of Heister. The common hepatic and bile duct is normally about 10–15 cm long and 5 mm wide, in which the hepatic bile duct is roughly 4 cm long. The common bile duct merges with the pancreatic duct before entering the duodenum at the ampulla.

A 1D model of the human biliary system, shown schematically in Fig. 2, has been described by Li *et al.*[30] The common bile duct and the common hepatic duct are represented by straight circular rigid tubes. These tubes are connected to the gallbladder by an idealized cystic duct[36] at a T-junction. The valves of Heister in the cystic duct are replaced by equal-spaced staggered baffles, Fig. 2a. Two models of the idealized cystic duct were used: one with rigid wall and the other with compliant wall. The directions of the bile flow during gallbladder emptying, and refilling are shown in Figs. 2b and 2c, respectively. Usually, emptying takes about half an hour or longer and refilling up to 6 h (until the next meal).

Non-Newtonian Gallbladder Bile

The viscosity–shear rate relation of bile varies in different experiments and is clearly subject dependent. In this paper, we have chosen to use a generalized Carreau model with parameters estimated from experiments by Gottschalk and Lochner[21] and Coene *et al.*[13] The bile viscosity is calculated from Carreau's equation:

$$\mu = \mu_\infty + (\mu_0 - \mu_\infty)(1 + \lambda^2\gamma^2)^{\frac{m-1}{2}}, \qquad (1)$$

where μ_0 is the bile dynamic viscosity at zero shear rate, μ_∞ is the viscosity at infinite shear rate, λ is the time constant, γ is the shear rate, and m is the power. Carreau's equation has no singularities in either the low or high shear rate limits, and is widely used for general non-Newtonian fluids. Figure 3 shows the experimental bile viscosity data of Gottschalk and Lochner[21] and Coene *et al.*,[13] together with our curve fitting with $\mu_0 = 10^{-2}$ Pa s, $\mu_\infty = 10^{-3}$ Pa s, $\lambda = 160.5742$ s, and $m = 0.4843$. The gallbladder bile density ρ is taken to be 1000 kg/m^3.[35] The two experiments do not agree closely with each other, hence we

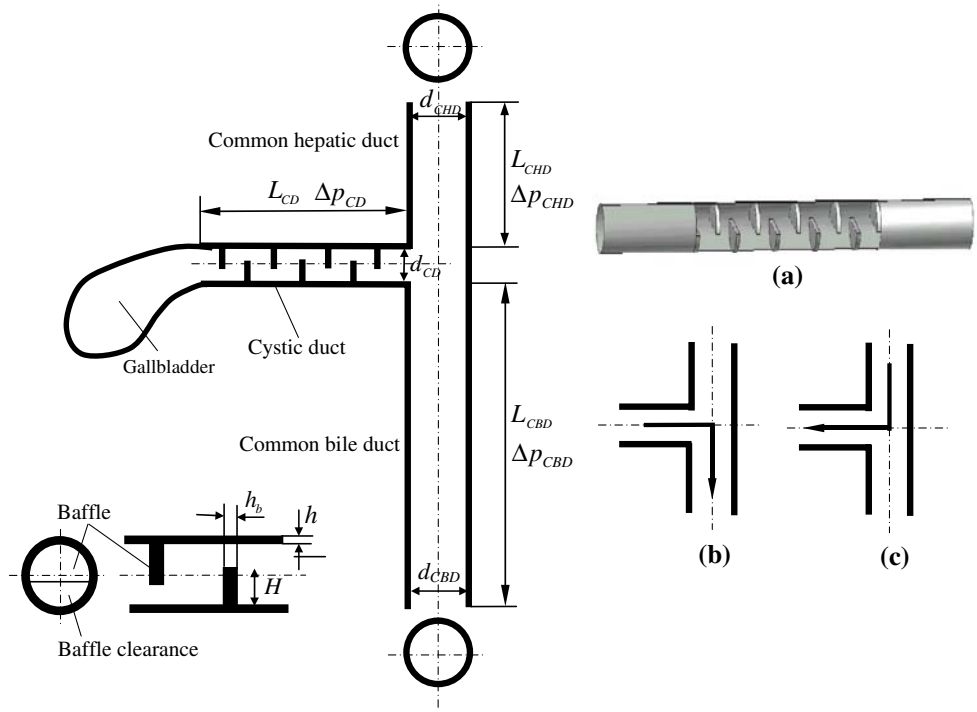

FIGURE 2. Schematic geometric model of the human biliary system, with (a) baffles in cystic duct, and bile flow directions in the (b) the emptying, and (c) refilling phases.

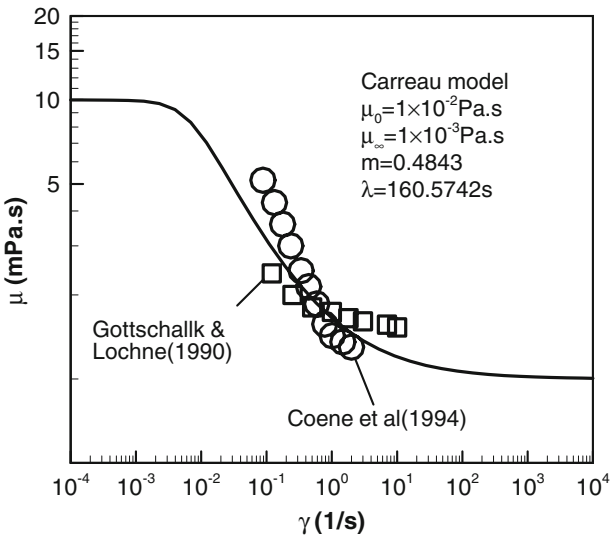

FIGURE 3. The Carreau model for non-Newtonian bile which fits both Coene *et al.*'s[13] and Gottschalk and Lochner's[21] experimental data of bile.

chose our curve to be approximate to both sets of data, and extending over a wider range of shear rate. We find that our qualitative results do not change with the choice of these parameters.

To examine the effect of the non-Newtonian bile, we also chose a Newtonian reference fluid with a dynamic viscosity equal to the non-Newtonian viscosity at the infinite shear rate $\mu = \mu_\infty$. This reference fluid has been used by previous workers.[11,12,20,34]

An Equivalent Tube for Cystic Duct

Following Li *et al.*,[30] we model the baffled tube with an equivalent straight tube. The effects of the equal-spaced staggered baffles on the flow in the idealized cystic duct are expressed in terms of an equivalent diameter, d_{eq}, and equivalent length, L_{eq}. The equivalent diameter is calculated from the diameter of the cystic duct, d_{CD}, the baffle cut area, A_1, and the number of baffles n:

$$d_{eq} = d_{min} + (d_{CD} - d_{min})\left(1 - \frac{n}{n_c}\right), \qquad (2)$$

where $d_{min} = 2\sqrt{A_1/\pi}$ (see Fig. 2), and n_c is the maximum number of baffles considered. More detail on how Eq. (2) is derived is given by Li *et al.*[30]

The equivalent tube length is determined from the actual distance traveled by the bile as it negotiates the baffles plus an extra length corresponding to minor losses in the baffle zone, i.e.

$$L_{eq} = H(n-1) + L_{CD} + L_k, \qquad (3)$$

where H is the baffle height (Fig. 2), L_{CD} is the length of the cystic duct, and L_k is the length representing minor flow losses due to sudden expansions and

contractions of the flow caused by the baffles. The length L_k is calculated from

$$L_k = \frac{d_{eq}\Delta p_k}{4\tau_w}, \tag{4}$$

where τ_w is the wall shear stress, and Δp_k represents the pressure losses due to bends, sudden expansion, and contraction.[5,30,47]

Fluid–Structure Interactions During the Emptying Phase

The pressure drop in the biliary system is due to the non-Newtonian bile flowing through the elastic cystic duct and the rigid common bile duct. At the beginning of emptying, the elastic cystic duct is assumed to be circular under an external pressure p_e (abdominal pressure). During emptying it may become partially collapsed toward the downstream end due to a decreased transmural pressure as bile flows. The governing equations for the fully developed, steady, Newtonian or non-Newtonian, laminar flow in the elastic cystic duct are[37,47]

$$Q = Au, \tag{5a}$$

$$\rho u\frac{du}{dx} = -\frac{dp}{dx} - \frac{4\tau_w}{d}, \tag{5b}$$

$$\frac{8Q}{\pi d^3} = \frac{1}{\tau_w^3}\int_0^{\tau_w} \gamma\tau^2 d\tau, \tag{5c}$$

where u is the bile velocity, d is the local internal diameter of the cystic duct and it is less than d_{eq} because of the duct collapse, τ is the shear stress, and $\tau = \tau_w$ at the tube wall, which can be calculated from Eq. (1) as $\tau = \mu\gamma$. For Newtonian flow, we have $\tau_w = 32Q\mu/\pi d^3$.

For a given flow rate, the pressure in the duct is obtained by integrating Eq. (5b) along the duct from the inlet, and is written as

$$p = p_{in} - 4\int_0^x \frac{\tau_w}{d}dx + \frac{1}{2}\rho Q^2\left(\frac{1}{A_{in}^2} - \frac{1}{A^2}\right), \tag{6}$$

where p is the internal pressure and p_e is the external pressure acting on the cystic duct. The inlet pressure is chosen as the reference pressure.

The constitutive equation for the elastic duct wall is chosen to be the 'tube law' for homogeneous elastic materials[9,37]:

$$p - p_e = \frac{Eh^3}{3(1-\kappa^2)d^2}(\alpha^k - \alpha^{-l}), \tag{7}$$

where $\alpha = A/A_{eq}$, $A_{eq} = \pi d_{eq}^2/4$ is the cross-sectional area of rigid tube, h is the wall thickness, and κ is the Poisson's ratio of the elastic wall. The parameters k and l are chosen to be 20, and 1.5, respectively, which are same as those used for other biological collapsible vessels.[37] E is the Young's modulus of the duct, chosen to be 300–500 Pa for the cystic duct at the pressure range investigated.[30]

Coupling Eqs. (6) and (7), we have the fluid–structure interaction (FSI) equation

$$p_{in} - 4\int_0^x \frac{\tau_w}{d}dx + \frac{1}{2}\rho Q^2\left(\frac{1}{A_{in}^2} - \frac{1}{A^2}\right) = p_e + \frac{Eh^3}{3(1-\kappa^2)d^2}(\alpha^k - \alpha^{-l}). \tag{8}$$

The boundary condition at the inlet is:

$$p_{in} = p_e + \frac{\pi^{3/2}Eh^3}{12(1-\kappa^2)A_{in}^{3/2}}\left(\alpha_{in}^k - \alpha_{in}^{-l}\right), \tag{9}$$

where $\alpha_{in} = A_{in}/A_{eq}$ is the cross-sectional area ratio at the tube inlet and p_e is the external pressure, which is set to be zero.

Equation (8) represents a boundary value problem, which may be solved for $A(x)$ using a finite difference method with the aid of Eq. (5c) for given E, A_{eq}, and Q. The fluid pressure can be obtained from Eq. (6). The pressure drop in the cystic duct is thus

$$\Delta p_{CD} = p_{in} - p_{out}. \tag{10}$$

The pressure drop for the rigid common bile duct during emptying is given by

$$\Delta p_{CBD} = \frac{4L_{CBD}\tau_w}{d_{CBD}} + \Delta p_{te}, \tag{11a}$$

$$\frac{8Q}{\pi d_{CBD}^3} = \frac{1}{\tau_w^3}\int_0^{\tau_w} \gamma\tau^2 d\tau, \tag{11b}$$

where Δp_{te} accounts for the pressure losses at the T-junction. These losses are due to flow rounding a 90° bend and expanding from the smaller cystic duct to the larger common bile duct. These two losses can be estimated from

$$\Delta p_{te} = 16c_4\frac{\rho Q^2}{\pi^2 d_{CD}^4} + 16c_2\frac{\rho Q^2}{\pi^2 d_{CD}^4}, \tag{12}$$

with $c_2 = (1 - A_{CD}/A_{CBD})^2$, $c_4 = 0.75$.[5,30] Thus the total pressure drop in the biliary system during emptying is

$$\Delta p_{EM} = \Delta p_{CD} + \Delta p_{CBD}. \tag{13}$$

Pressure Drop During the Refilling Phase

Figure 2c shows that during refilling the bile flows from the liver to the common hepatic duct and enters the gallbladder via the cystic duct. Since the flow of hepatic bile is very small and the refilling time is at least three times longer than that of emptying, the cystic duct and common hepatic duct walls may be assumed to be rigid. Thus the pressure drop Δp_{RF} during refilling is

$$\Delta p_{RF} = \Delta p_{CD} + \Delta p_{CHD}, \tag{14}$$

where Δp_{CD} is the pressure drop in the cystic duct with a rigid wall

$$\Delta p_{CD} = \frac{4L_{eq}\tau_w}{d_{eq}}, \tag{15a}$$

with τ_w computed from

$$\frac{8Q}{\pi d_{eq}^3} = \frac{1}{\tau_w^3}\int_0^{\tau_w} \gamma\tau^2 d\tau. \tag{15b}$$

The pressure drop in the common hepatic duct is

$$\Delta p_{CHD} = \frac{4L_{CHD}\tau_w}{d_{CHD}} + 16c_4\frac{\rho Q^2}{\pi^2 d_{CD}^4} + 16c_2\frac{\rho Q^2}{\pi^2 d_{CD}^4}, \tag{16a}$$

where

$$\frac{8Q}{\pi d_{CHD}^3} = \frac{1}{\tau_w^3}\int_0^{\tau_w} \gamma\tau^2 d\tau. \tag{16b}$$

Q–τ_w Relationship

For a given flow rate, to obtain the corresponding pressure drop, first we need to evaluate τ_w. For a non-Newtonian flow, the inverse problem needs to be solved: for a given value of Q, τ_w is to be determined from Eqs. (1) and (5c), since in non-Newtonian flow τ_w is no longer proportional to Q. Figure 4 shows the nonlinear $Q/\pi d^3$–τ_w relationship for the shear rate γ in the range of 0–500 s^{-1}, which covers the full physiological range in the biliary system. The corresponding linear Newtonian Q–τ_w relationship is also shown in Fig. 4 for comparison.

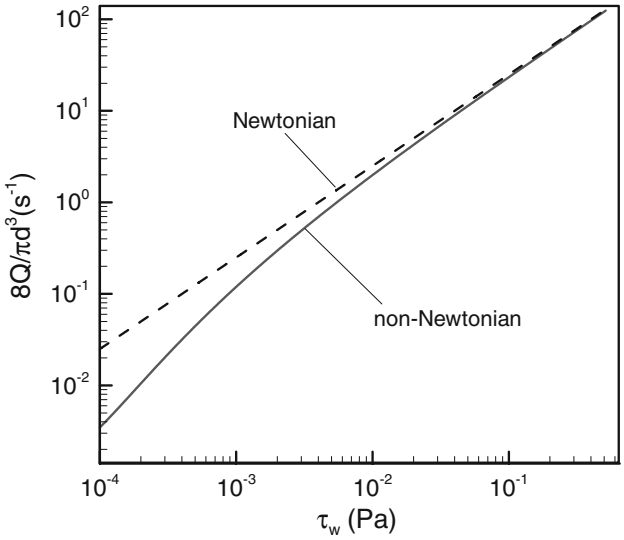

FIGURE 4. $Q/\pi d^3$ as a function of τ_w with Carreau's model (solid), and the corresponding Newtonian model (dashed).

3D MODEL FOR CYSTIC DUCT WITH FLUID–STRUCTURE INTERACTIONS

3D Model

To obtain detailed non-Newtonian flow patterns in the cystic duct and to validate the 1D model, numerical simulations of 3D flow in an elastic cystic duct were carried out using ADINA 8.4.[1] The cystic duct wall is assumed to be a linearly elastic, isotropic and homogenous material. The governing equations for the steady, laminar flow of the bile are

$$\frac{\partial u_i}{\partial x_j} = 0, \tag{17a}$$

$$\rho u_j\frac{\partial u_i}{\partial x_j} = -\frac{\partial p}{\partial x_j} + \frac{\partial \tau_{ij}}{\partial x_j}, \tag{17b}$$

where τ_{ij} ($i, j = 1, 2, 3$) is the shear stress in flow field and is related to the shear strain rate, ε_{ij}, and the dynamic viscosity of bile, μ. The constitutive equations are

$$\tau_{ij} = 2\mu\varepsilon_{ij}, \tag{18a}$$

$$\varepsilon_{ij} = \frac{1}{2}\left(\frac{\partial u_i}{\partial x_j} + \frac{\partial u_j}{\partial x_i}\right), \tag{18b}$$

where for the Newtonian fluid, $\mu = \mu_\infty$, and for the non-Newtonian bile, the viscosity μ depends on the shear rate $\gamma\left(\gamma = \sqrt{2\varepsilon_{ij}\varepsilon_{ji}}\right)$, and is given by Eq. (1).

As the 3D FSI simulations are extremely time consuming, we focus on just one idealized cystic duct, which has six uniformly staggered baffles. The inner diameter of the cystic duct is $d_{CD} = 5$ mm, the wall thickness is $h = 1$ mm, and baffle thickness is $h_b = 1$ mm. Because the thickness/radius ratio is $2h/d_{CD} = 0.4$, which cannot be modeled as a thin shell structure, we model the cystic duct wall as 3D elements in ADINA 8.4.[45] A steady, 3D, laminar bile flow is applied at the duct inlet. The duct is subject to an external pressure, p_e, and it is either deformed or collapsed under the transmural pressure, $p - p_e$. Here we

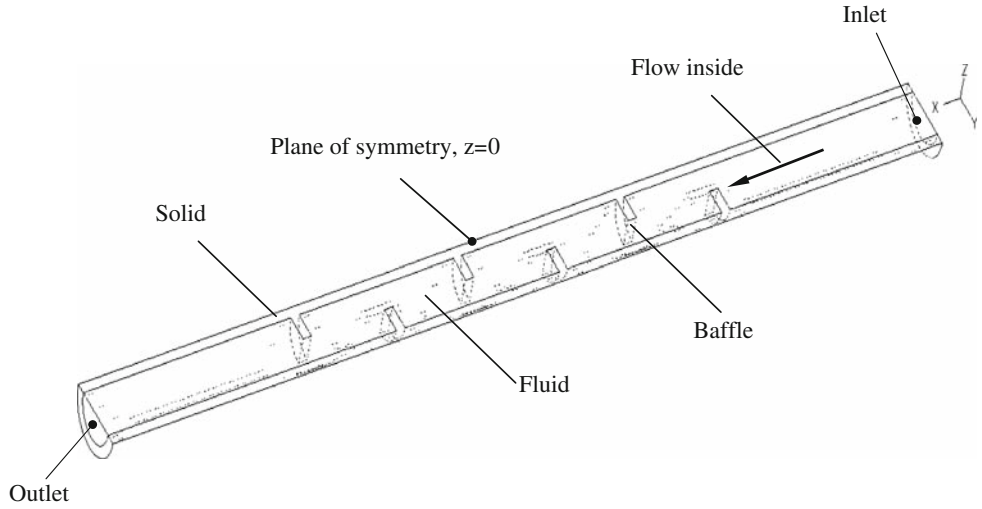

FIGURE 5. The 3D cystic duct model (half) for the FSI analysis. The duct has six uniform staggered baffles.

assume that p_e is equal to the fluid pressure at the duct inlet, p_{in}. Due to the symmetry in geometry, only half the duct is modeled (Fig. 5).

Numerical Methods

In the 3D model the coupled fluid and structural problems are solved individually using an iterative method[48]; the link between the fluid and structure is then realized with data transfer across the interface. A fully coupled and convergent solution is achieved by iterating to convergence between fluid and structure at each time step. One drawback of using such an iterative method is that it is extremely demanding on computational resources. To handle the moving interface between fluids and solids, an arbitrary Lagrangian–Eulerian (ALE) formulation is applied to the fluid flow governing equations where the moving mesh velocity vector is included. The traction equilibrium and displacement compatibility are satisfied at the interface.

Fluid and Solid Models

In the 3D computations, both Newtonian and non-Newtonian fluids are considered. The cystic duct wall and baffles are assumed to be a homogenous, isotropic elastic solid material with the density of 1020 kg/m^3 and the Poisson ratio, $\kappa = 0.45$, is chosen to reflect the incompressibility of the soft tissue. The relationship between stress and strain is linear. Although different values of the Young's modulus can be studied, we have found that it is difficult to obtain a converged solution with ADINA 8.4 for $E < 500$ Pa (due to numerical difficulties because of mesh distortions), hence we choose $E = 500$ Pa in the 3D FSI simulations.

Boundary Conditions

For the bile flow, the normal traction conditions are applied at the cystic duct inlet and outlet, respectively. At the inlet, the normal traction is zero. At the outlet, it is set to lie between the range of: -0.02 to -3.5 Pa, the magnitude of which determines the pressure drop, since the inlet pressure is set to be zero. The range of the pressure drop is estimated from the previous 1D study, which corresponds more or less to a Reynolds number range of 0–40.[30] In the plane of symmetry, the velocity component in the z direction is chosen to be zero.

For the solid structure (Fig. 5), the displacement in the x direction at the cystic duct inlet and the outlet is chosen to be zero. The displacement in the z direction and the rotation about the x and y axes are zero in the plane of symmetry. To eliminate rigid body motion, the y displacements of the inlet and outlet points on the outside surface of the cystic duct, which have the lowest z coordinates, are fixed to be zero. As in the 1D model, zero pressure is applied on the outside surface of the duct, i.e. $p_e = 0$.

For the elastic duct, the interface between bile and the inner side of the cystic duct is set to be the fluid–structure interface where a no-slip velocity condition is applied.

Discretization of the Solid and Fluid Domains

The four-node tetrahedral element is used to discretize the fluid and structure domain. It is a linear element with first order accuracy in the spatial interpolations. To choose the optimal grid points, we first carried out the numerical scheme and grid independence tests for the rigid cystic duct and the Newtonian fluid.

To investigate the computational accuracy of ADINA 8.4, we compare the result in terms of pressure

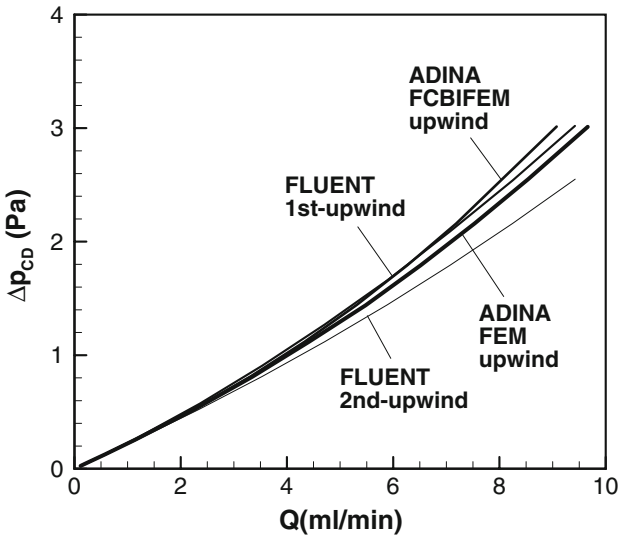

FIGURE 6. Pressure drop vs. flow rate for the 3D rigid cystic duct, calculated using various numerical schemes.

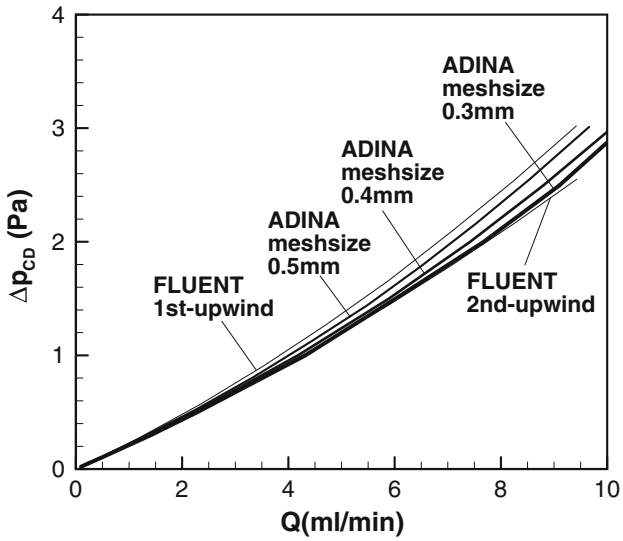

FIGURE 7. Pressure drop vs. flow rate for the rigid cystic duct, calculated for various grid sizes. The higher thin line is the result using FLUENT first-order upwind, and the lower thin line is using FLUENT second-order upwind, and the dark lines are using ADINA for different meshes.

drop with another commercial package FLUENT 6.2,[19] which has a well-tested fluid solver (but, unlike ADINA, it cannot be used to solve fluid–structure interaction (FSI) problems). The comparisons are shown in Fig. 6. The same mesh size (0.5 mm) is used in both cases. Both first- and second-order upwind schemes for the convection term in the Navier–Stokes equations are applied in FLUENT. These are compared with the FEM upwind and FCBI FEM (flow-condition-based interpolation finite element method) upwind schemes in ADINA. Figure 7 shows a noticeable difference in the pressure drop between the first- and second-order schemes in FLUENT. Both FEM and FCBI FEM upwind schemes in ADINA give results closer to the first-order scheme of FLUENT, with FEM slightly better than FCBI FEM[1]. Since FLUENT does not have FSI capabilities, only ADINA with FEM upwind scheme is used for the following FSI computations.

We present the results for a number of different grids. The pressure drops obtained from three different meshes with mesh size of 0.5, 0.4, and 0.3 mm are shown in Fig. 7. These results are again compared with those calculated using FLUENT. It can be seen that the pressure drops given by ADINA for different mesh sizes are confined within the range of the pressure drops calculated by FLUENT. Moreover, as the mesh size gets small, the result from ADINA approaches the more accurate second-order upwind result in FLUENT. Therefore, the 0.3 mm mesh was used in the fluid domain giving rise to a total of 180,000 fluid elements.

[1]ADINA's second-order upwind scheme can be achieved by using the FCBI-C element, which, however, converges slowly for the deformed domain problems.

TABLE 1. Effect of mesh size of the solid domain.

Mesh size (mm)	Q (L/s)	Re_{CD}	α_{out}	f/f_0
1.00	9.763	41.43	0.9631	3.016
0.75	9.760	41.42	0.9633	3.017
0.45	9.756	41.41	0.9633	3.018

The effect of mesh size of the solid domain on the results is shown in Table 1 for meshes of 1.0, 0.75, and 0.45 mm. This test is carried out for a fluid mesh size of 0.3 mm and a pressure drop of 3.0 Pa. It is clear that these results agree to three significant digits in all these cases. In the subsequent calculations, a solid mesh size of 0.45 mm was used, requiring 52,000 solid elements in total.

RESULTS

Unless otherwise stated, the computational parameters used in the following results are given in Table 2. In this section, we first present results from the 1D model, followed by results from 3D simulations. The comparison of the results between 1D and 3D models are given towards the end.

Pressure Drop in the Biliary System—1D Predictions

The pressure drop across the biliary system, i.e. the cystic duct with the common bile duct during emptying, and cystic duct with the hepatic duct during refilling (see Fig. 1), predicted using the 1D model is

TABLE 2. Selected parameters for human biliary system and bile.

Cystic duct	d_{CD} = 1–6 mm, L_{CD} = 40 mm, $h = h_b$ = 0.5 mm, ξ = 0.3–0.7, n = 0–10, E = 300–500 Pa
Common bile duct	d_{CBD} = 6 mm, L_{CBD} = 100 mm
Common hepatic duct	d_{CHD} = 6 mm, L_{CHD} = 40 mm
Bile	ρ = 1000 kg/m^3
	For the Newtonian fluid, $\mu = 1 \times 10^{-3}$ Pa s
	For the non-Newtonian fluid, $\mu_0 = 1 \times 10^{-2}$ Pa s
	$\mu_\infty = 1 \times 10^{-3}$ Pa s, m = 0.4843, λ = 160.5742 s, Carreau model

shown in Fig. 8b. This pressure drop is calculated from a given flow rate estimated from a measured volume history during emptying and refilling.[39] The estimated flow rate $Q = dV/dt$ during emptying and refilling is shown in Fig. 8a. Since the refilling is much longer than the emptying, just a part of refilling is shown in the figure. It is clear that the pressure drop is considerably smaller (<3 Pa) during refilling, as the direction of flow is reversed.

As in the Newtonian model,[30] the effect of the elastic cystic duct is to increase the pressure drop in the non-Newtonian model. This is due to narrower diameters with a partially collapsed cystic duct during emptying. In both the rigid and elastic models, the non-Newtonian bile also requires a greater pressure drop to drive the flow, especially during the emptying phase. The pressure drop in cystic duct is the major part of the pressure loss in the biliary system, with less than 1.5% of the pressure drop occurring in the common bile duct, and less than 0.15% of the pressure drop in the common hepatic duct. Therefore in the following we will focus on flow features in the cystic duct only.

Darcy Friction Factor of Cystic Duct—1D Predictions

The Darcy friction factor, f, a commonly used nondimensional measure of the pressure drop in duct flow[46] is defined as

$$f = \left(\frac{2d_{eq}}{L_{eq}\rho u^2}\right)\Delta p_{CD}. \tag{19}$$

To demonstrate the effects of the variation in the duct geometry, the Darcy friction factor ratio f/f_0 is used, where f_0 (= Re/64) is the Darcy friction factor for a Newtonian laminar flow in a rigid duct. The Reynolds number is

$$\mathrm{Re} = \frac{4\rho Q}{\pi \mu_\infty d_{eq}}. \tag{20}$$

This definition only makes sense for the Newtonian fluid, since the dynamic viscosity is not a constant for the non-Newtonian fluid. Therefore, the Reynolds number is used only as an indication of the flow rate for both Newtonian and non-Newtonian fluids, so that a comparison can be made. For a given geometry, the Reynolds number cannot indicate flow similarity between the Newtonian and non-Newtonian flows.

The ratio f/f_0 vs. Re is plotted for various parameters of a rigid model in Fig. 9, for Newtonian and non-Newtonian fluids. The changes in the cystic duct geometry are expressed in terms of the cystic duct diameter, the number of baffles, and the dimensionless baffle height. The non-Newtonian bile always causes a larger pressure drop than that of the Newtonian fluid, especially for a more complicated geometry (i.e. with

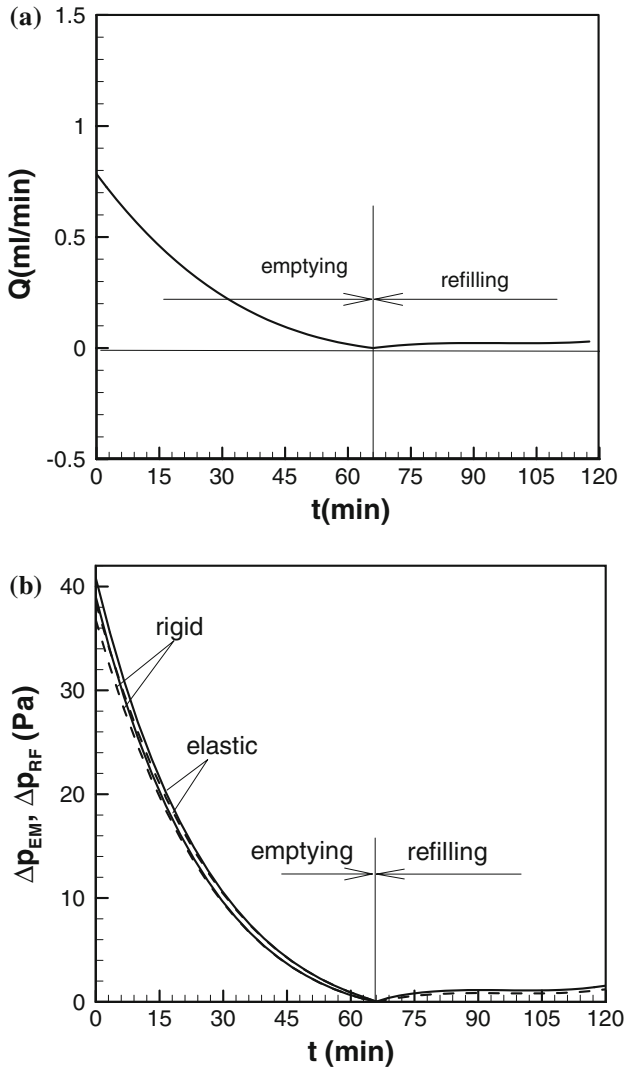

FIGURE 8. Bile flow rate (a) and pressure drop (b) of a human biliary system during emptying and refilling for the non-Newtonian (solid line) and Newtonian fluids (dashed line), for d_{CD} = 1 mm, ξ = 0.5, n = 6, α_{in} = 1, and E = 300 Pa. All other parameters are listed in Table 2.

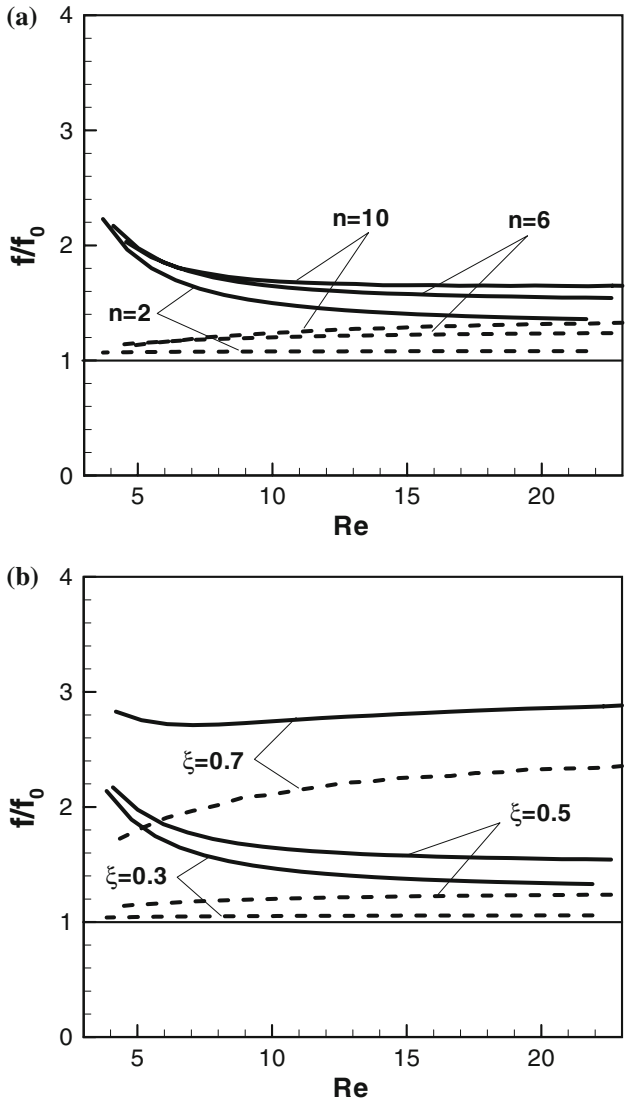

FIGURE 9. Rigid model: f/f_0 against Re for the non-Newtonian (solid line) and Newtonian (dashed line) fluids, with L_{CD} = 40 mm, Q = 1 mL/min, and (a) n = 2, 6, and 10; (b) ξ = 0.3, 0.5, and 0.7.

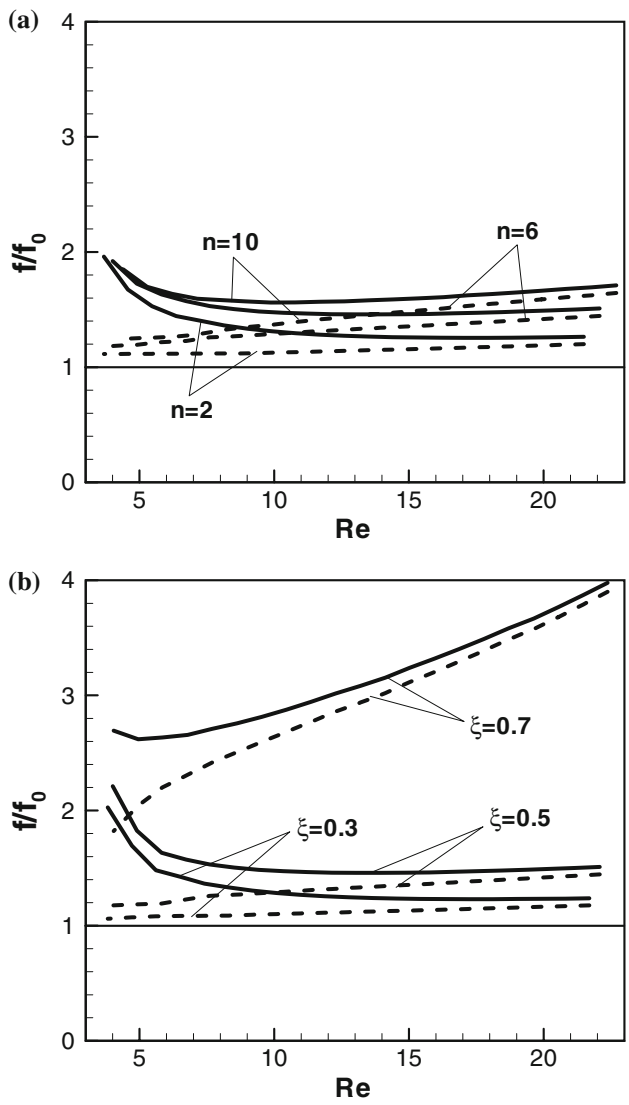

FIGURE 10. Elastic model: f/f_0 against Re for the non-Newtonian (solid line) and Newtonian (dashed line) fluids, with L_{CD} = 40 mm and Q = 1 mL/min, E = 300 Pa, and (a) n = 2, 6, and 10; (b) ξ = 0.3, 0.5, and 0.7.

higher or more baffles). The most significant difference is that for Newtonian bile, f/f_0 decreases with Re, while the opposite is observed for the non-Newtonian bile. This is because in our study the flow rate Q is kept constant. For the non-Newtonian fluid, the shear rate is reduced, due to an increased d_{eq} as Re decreases (see Eq. 20). This, in turn, increases the dynamic viscosity μ according to the Carreau's model (Eq. 1). Moreover, significant difference of f/f_0 between Newtonian and non-Newtonian flows can be observed. The lower the Reynolds number (larger d_{eq}), the higher the value of f/f_0 in the non-Newtonian fluid. The reason for this is the significantly increased dynamic viscosity of non-Newtonian fluid due to an increased diameter or decreased Re (with constant flow rate).

The same results, but for the elastic wall cystic duct, are shown in Fig. 10. Compared with the rigid duct flow, a smaller difference between the Newtonian and non-Newtonian fluids is observed, especially at a higher Reynolds number. This is because the collapse of the elastic duct narrows the tube diameter, thus increasing the shear rate and decreasing the dynamic viscosity. Therefore, the non-Newtonian behavior may become less significant for a deformable elastic duct.

It is noted that for both Newtonian and non-Newtonian flows, the dimensionless baffle height has a more dominant effect on f/f_0 than the baffle number n.

Detailed Flow Pattern in the 3D Model

Although the 1D model predicts the pressure drop reasonably well, it cannot show the detailed flow pattern in the cystic duct. By carrying out the 3D simulations, we are able to present some detailed flow fields and wall deformation. In these results, the Reynolds number is now defined with respect to the cystic duct diameter ($Re_{CD} = 4\rho Q/\pi\mu_\infty d_{CD}$); since the baffles are taken into account fully in the 3D models, no equivalent diameter is required. For lower Reynolds numbers, the wall deformation in the elastic cystic duct is small, and there are no significant differences in the flow patterns between a rigid and elastic duct (Fig. 11). However, when Re is higher, the elastic cystic duct collapses at the downstream end, causing the narrowing of the lumen, and the wall deformation is more noticeable; see Fig. 11 for $Re_{CD} = 20$. The difference is slightly more in the non-Newtonian case. Compared with the un-deformed configuration, the maximum wall displacement at the baffle tip is about 6.43% (Newtonian) and 7.14% (non-Newtonian) at $Re_{CD} = 3.5$, and 27.14% (Newtonian) and 28.57% (non-Newtonian) at $Re_{CD} = 20$, respectively.

Flow patterns in the rigid and elastic ducts are shown in Fig. 12 for $Re_{CD} = 3.5$. Flow patterns in the corresponding rigid cystic duct are similar (not shown) as the elastic deformation is small for this case. Flow separation is very weak; however both the peak forward and reversed velocities are slightly higher in the Newtonian flow (about 2.893 and −0.011 mm/s), than the non-Newtonian flow (2.792 and −0.000237 mm/s). For the elastic ducts, similar differences between Newtonian and non-Newtonian fluids are observed. In addition, due to the elastic collapsing at the downstream end, as shown in Fig. 11, the deformation of the elastic cystic duct makes the lumen narrower, which in turn introduces extra viscous dissipation. As a result, the pressure drop increases, and the velocity increases at the boundary layers near the tip of the baffles. The peak velocity increases from 2.893 mm/s (rigid) to 3.066 mm/s (elastic) for Newtonian, and 2.792 mm/s (rigid) to 2.952 mm/s (elastic) for non-Newtonian flow.

The velocity vector fields at a higher $Re_{CD} = 20$ are shown in Fig. 13 for both rigid and elastic ducts. There is a clear flow separation zone in both cases, which is again slightly stronger in the Newtonian flow. For the rigid duct, the peak reversed (negative) velocity is about 3.934 mm/s in the Newtonian fluid, and 2.136 mm/s in the non-Newtonian fluid. For the elastic duct: the peak forward velocity increased from 15.50 mm/s (rigid) to 18.54 mm/s (elastic) in the Newtonian case, and 15.49 mm/s (rigid) to 16.18 mm/s (elastic) in the non-Newtonian case. However, although the peak reversed

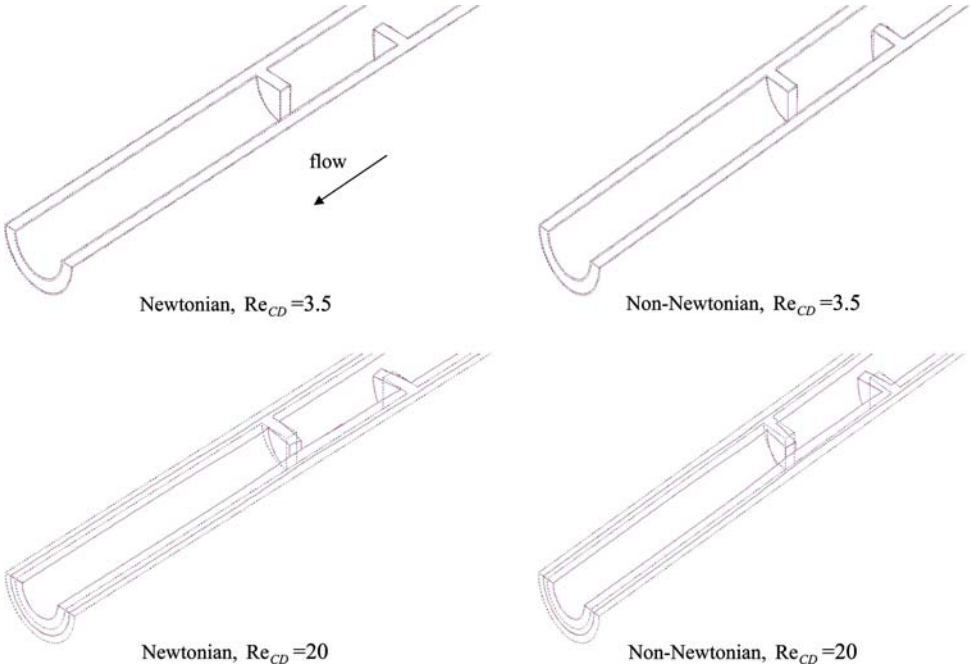

FIGURE 11. Comparison of the configuration between the original (dashed) and the deformed (solid) cystic duct for the Newtonian and non-Newtonian bile at Reynolds numbers $Re_{CD} = 3.5$ and 20, respectively. The displacement magnification factor is 30 for all plots. At $Re_{CD} = 3.5$, there is no noticeable difference between the two configurations. However, at $Re_{CD} = 20$, a significant deformation is shown in Newtonian flow and even more so for non-Newtonian flow. Only part of the distal end (outlet) of the cystic duct is shown.

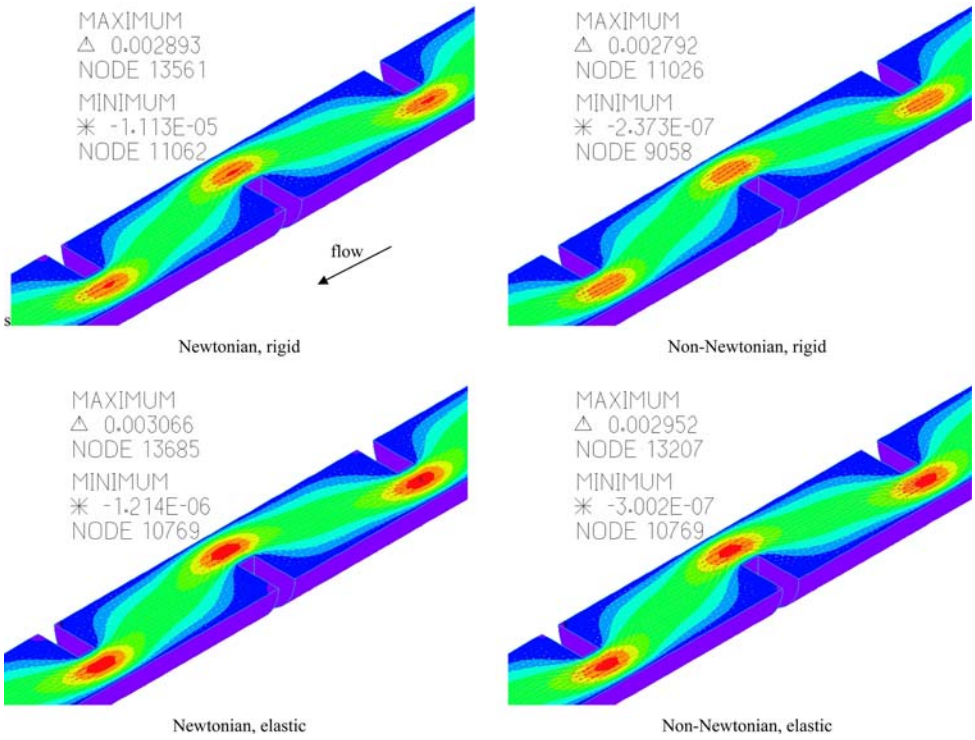

FIGURE 12. Velocity vector field and axial velocity contour of the Newtonian and non-Newtonian fluids in the rigid and elastic cystic ducts at $Re_{CD} = 3.5$. The flow separation is present but very weak in all four cases, and is slightly greater in the Newtonian flow. Only part of the distal end (outlet) of the cystic duct is shown.

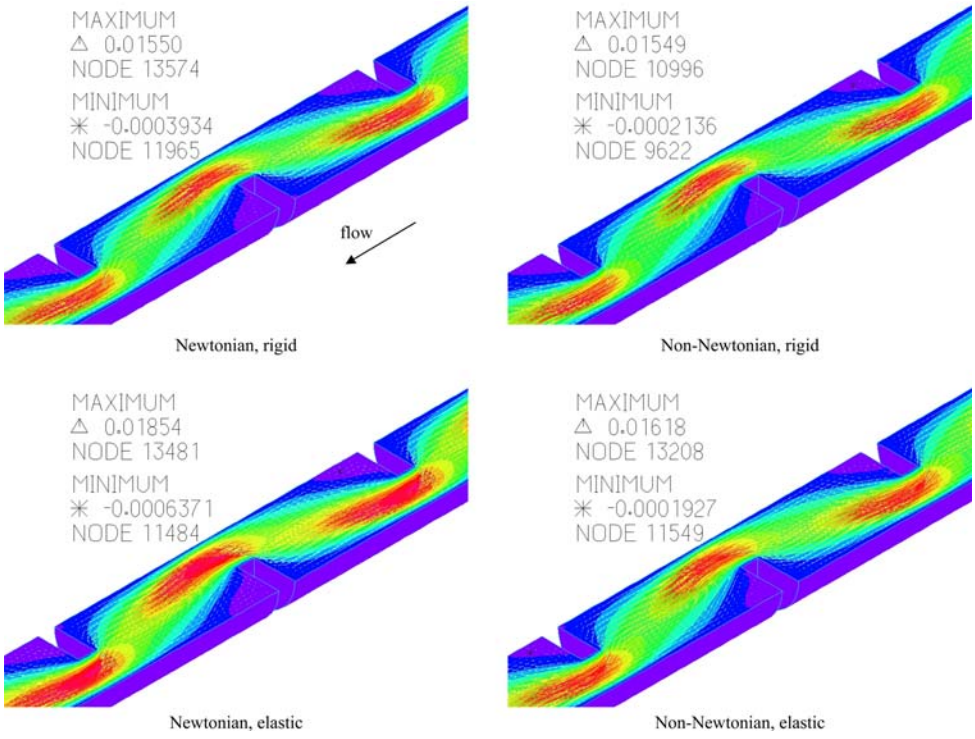

FIGURE 13. Velocity vector field and axial velocity of the Newtonian and non-Newtonian flows in the rigid and elastic cystic ducts at $Re_{CD} = 20$. The flow separation is present in four cases, and is stronger than the cases with $Re_{CD} = 3.5$. Only part of the distal end (outlet) of the cystic duct is shown.

velocity is almost doubled for the Newtonian case: from −0.3934 mm/s (rigid) to −0.6371 mm/s (elastic), this is not observed for the non-Newtonian case. This is because the slow reversed flow in the separated flow region (low shear rate or "dead water" zone) tends to be suppressed by the higher viscosity of the non-Newtonian bile. This relatively high viscosity at low shear rates is also responsible for the greater pressure drop in the non-Newtonian bile, as shown in section "Pressure Drop in the Biliary System—1D Predictions".

Stress Distributions in the 3D Elastic Cystic Model

We recently reported that gallbladder pain may be strongly related to the normal stress inside the gallbladder.[30] If the same pain receptors are located in the cystic duct, then the normal stress distribution inside the cystic duct may also be important. Here, we present the normal stress caused by the bile flow of the elastic cystic duct for both Newtonian and non-Newtonian flow at $Re_{CD} = 20$. Figure 14 (left) shows that the normal stress is highest around the baffle tips, and the maximum value (17.50 Pa) occurs at the last baffle tip closest to the distal end. Similar behavior is observed in non-Newtonian flow, though the maximum value is slightly higher, about 18.53 Pa.

The maximum shear stress distributions are shown in Fig. 14 (right). Since the maximum shear stress occurs at the wall, the maximum value of the maximum shear stress is the same as the maximum wall shear stress. Again, the maximum shear stress concentration is located around the baffle tip closest to the distal end, with the maximum value of 7.085 Pa for Newtonian flow, and 7.803 Pa for non-Newtonian flow. Although there are clear differences between flow patterns of Newtonian and non-Newtonian flows, the maximum shear stress distributions in the cystic duct wall are not significantly different at $Re_{CD} = 20$.

We also note from the 3D simulations that the bile dynamic viscosity of the non-Newtonian fluid varies in the flow field, the peak viscosity being in the area with the lowest shear rate which is located at each corner between a baffle and duct wall. The bile dynamic viscosity's value is between 1.074×10^{-3} and 1.0×10^{-2} Pa s. This is in contrast to the constant viscosity of 1×10^{-3} Pa s used in the entire flow field of Newtonian fluid.

Comparison Between 1D and 3D Models

The pressure drop predicted using the 1D model is compared with that of the 3D model, for Newtonian and non-Newtonian bile, and for rigid and elastic cystic ducts in Fig. 15. Here, the flow rate is chosen to be in the range of 0.12–9.42 mL min^{-1}, corresponding to a maximum Reynolds number of 40, based on cystic duct diameter $d_{CD} = 5$ mm.[36] Good agreement is achieved for all cases considered, Newtonian and non-Newtonian

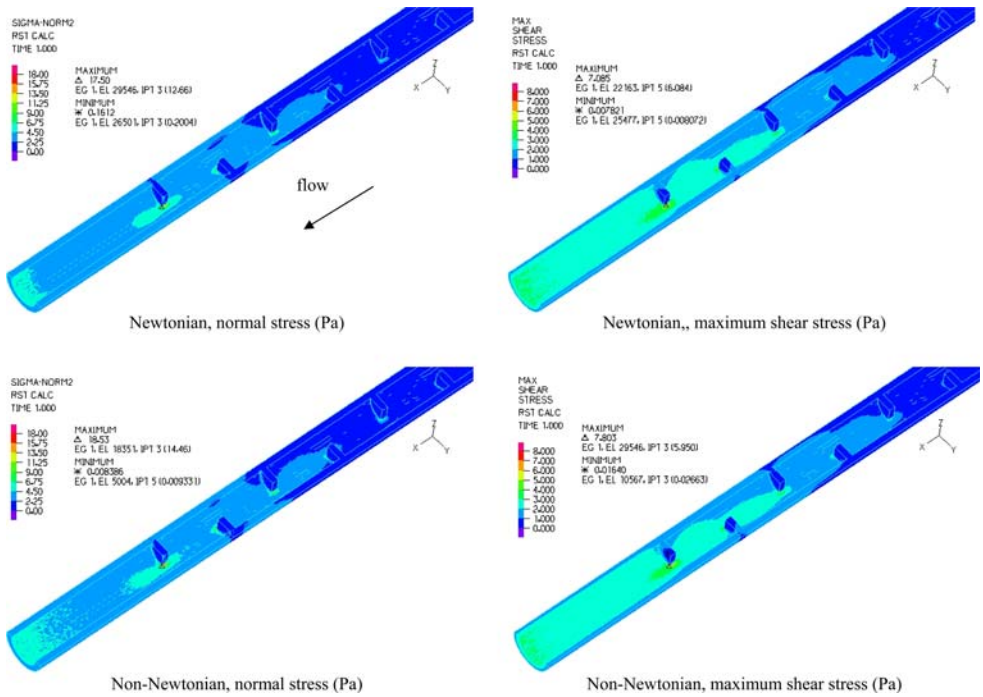

FIGURE 14. The normal stress (left) and the maximum shear stress (right) distributions in the elastic model for the Newtonian and non-Newtonian flows at $Re_{CD} = 20$. The maximum value of the stress is shown as the triangle at the tip of the first baffle. Only part of the distal end (outlet) of the cystic duct is shown.

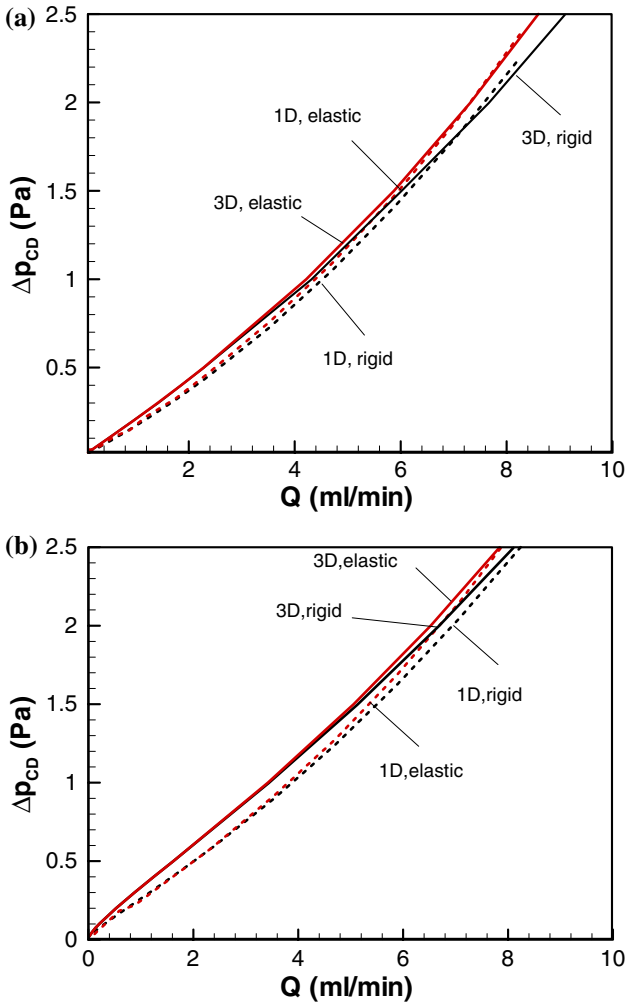

FIGURE 15. Pressure drop vs. bile flow rate for the Newtonian (a) and non-Newtonian (b) flows in the cystic duct. The solid line is from the 3D model, and dashed line is from the 1D model.

TABLE 3. Comparison between pressure drops predicted by 1D and 3D models.

	Pressure drop (Pa), $Q = 4.7$ mL/min, $Re_{CD} = 20$			
	Newtonian bile		Non-Newtonian bile	
Model	Rigid	Elastic	Rigid	Elastic
1D	1.05	1.09	1.24	1.27
3D	1.11	1.15	1.37	1.39

bile, rigid and elastic ducts, with a small discrepancy between the 3D and 1D models. Table 3 provides a more explicit comparison at $Q = 4.7$ mL/min, equivalent to $Re_{CD} = 20$. The difference between the pressure drop predicted by the 1D and 3D models for Newtonian bile is about 5% for both the rigid and the elastic cystic ducts, and about 10% for non-Newtonian bile in both rigid and elastic ducts. These results suggest that when pressure drop is required, the present 1D model would be able to predict it as well as the 3D model but with considerably reduced cost and turn round time, which may enable it to be used as a clinical diagnostic aid.

DISCUSSION

In this study, we found that for a normal cystic duct, if the bile is non-Newtonian as presented here, then the flow resistance is higher than that of Newtonian bile for a given flow rate. This means that the volume of bile emptied from the gallbladder is reduced for a given pressure drop. Such non-Newtonian behavior of the bile would enhance the bile stasis, a necessary condition for gallstone formation.[2] The effect of the non-Newtonian behavior becomes more significant for a lower Reynolds number.

The fact that the difference between 1D and 3D models is within 10% of the pressure drop is encouraging, as the 1D model is much faster and less demanding on computer resources and it is more feasible to extend it to include the whole biliary system. Therefore, if the pressure drop (or flow resistance) is of primary concern, then the 1D model is more useful for development as an aid in clinical diagnosis. For detailed stress predictions, the 1D model is of limited value. The maximum normal stress predicted by 3D elastic models are about 18.53 Pa (non-Newtonian), and 17.50 Pa (Newtonian); however, in 1D models these are only about 3.19 Pa (non-Newtonian), and 2.75 Pa (Newtonian).[2]

In addition to a greater pressure drop, the increased peak shear stress is also an indicator of more resistance to bile flow in the cystic duct, which will enhance bile stasis. Our 3D bile flow simulation results show that the peak shear stress occurs at the baffle tips and opposite duct wall areas. For the rigid cystic duct, the peak shear stress of the non-Newtonian fluid is about 7.8 Pa compared to 7.08 Pa for the Newtonian bile at $Re_{CD} = 20$. However, using the 1D model, the peak shear stress of Newtonian bile is predicted to be only 0.011 and 0.0088 Pa, for non-Newtonian and Newtonian flows, respectively. Again, this is a dramatic under estimation of the shear stress by the 1D model, and because the detailed stress distributions are very sensitive to the geometric changes and the peak stresses are all present around the baffle tips. In 1D models, these geometric details are lost by assuming an equivalent circular cylinder. Although the pressure losses due to the baffles are considered in the 1D model, it

[2]Calculated based on $\sigma = \Delta P d/2h$, where σ is the circumferential normal stress and ΔP is the pressure drop.

cannot be used to explore more detailed stress distributions in the biliary system.

The physiological and clinical applications of this work are in (i) cholelithiasis and (ii) assessing and understanding gallbladder pain. Incomplete drainage of the gallbladder may occur when the resistance to flow is too high; this requires further study. Preliminary work by us[29,31] suggests a correlation between pain and mechanical stresses of the biliary system, and this paper indicates that non-Newtonian effects will contribute to these stresses.

Finally, we should point out that one limitation of this study is that, in the absence of experimental data, we have assumed that the cystic duct is made of a homogenous isotropic linear elastic material. However, the tube law is nonlinear because of the geometry of the duct. Since the qualitative trend for all tube laws is similar, i.e. a flatter slope immediately after collapse sandwiched by two steeper slopes in the transmural pressure and cross-sectional area space, the observations from our study should not be qualitatively affected by imposing a different tube law. Nevertheless, future work is required to estimate the importance and influence of the nonlinearity and anisotropy on the stress calculations.

CONCLUSION

In this paper, we studied the pressure drop, flow pattern, and stress distributions in the human cystic duct models. Both 1D simplified model and 3D extensive numerical modeling of fluid–structure interactions have been presented. The bile was considered as a Carreau-type non-Newtonian fluid based on the existing experimental data. The effects of bile flow rate, number of baffles, and dimensionless baffle height on the Darcy friction factor were examined for the cystic ducts with diameter of 1–6 mm, of 2, 6, and 10 baffles and dimensionless baffle heights of 0.3, 0.5, and 0.7. The results show that the pressure drop across the cystic duct is increased due to non-Newtonian bile behavior compared with that of the Newtonian one. This difference becomes more significant if the compliance of the cystic duct is included in the modeling. The results of the 1D and 3D models, in terms of the pressure drop, agree very well for all cases considered, although the 1D model cannot be used to obtain accurate stress distributions inside the cystic duct.

ACKNOWLEDGMENT

XYL would like to acknowledge a Global Research Award from the UK Royal Academy of Engineering.

REFERENCES

[1]ADINA Theory and Modelling Guide, Vols. 1–3. Watertown, MA: ADINA R&D Inc., 2003.
[2]Bateson, M. Gallbladder disease. *Br. Med. J.* 318:1745–1748, 1999.
[3]Bertram, C. D., and N. S. J. Elliott. Flow-rate limitation in a uniform thin-walled collapsible tube, with comparison to a uniform thick-walled tube and a tube of tapering thickness. *J. Fluids Struct.* 17:541–559, 2003. doi:10.1016/S0889-9746(02)00160-3.
[4]Bertram, C. D., and J. Tscherry. The onset of flow-rate limitation and flow-induced oscillations in collapsible tubes. *J. Fluids Struct.* 22:1029–1045, 2006. doi:10.1016/j.jfluidstructs.2006.07.005.
[5]Bober, W., and R. A. Kenyon. Fluid Mechanics. New York: John Wiley & Sons, pp. 295–297, 1980.
[6]Bouchier, I. A. D., S. R. Cooperband, and B. M. El Kodsi. Mucous substances and viscosity of normal and pathological human bile. *Gastroenterology* 49:343–353, 1965.
[7]Brower, R.W., and A. Noordergraaf. Pressure-flow characteristics of collapsible tubes: a reconciliation of seemingly contradictory results. *Ann. Biomed. Eng.* 1:333–355, 1973. doi:10.1007/BF02407674.
[8]Calvert, N. W., G. P. Troy, and A. G. Johnson. Laparoscopic cholecysterctomy: a good buy? *Eur. J. Surg.* 166:782–786, 2000. doi:10.1080/110241500447416.
[9]Cancelli, C., and T. J. Pedley. A separated-flow model for collapsible-tube oscillations. *J. Fluid Mech.* 157:375–404, 1985. doi:10.1017/S0022112085002427.
[10]Catnach, S. M., P. D. Fairclough, R. C. Trembath, L. J. D. O'Donnell, A. M. McLean, P. A. Law, and J. E. A. Wickham. Effect of oral erythromycin on gallbladder motility in normal subjects and subjects with gallstones. *Gastroenterology* 102:2071–2076, 1992.
[11]Chen, J., and X. Y. Lu. Numerical investigation of the non-Newtonian blood flow in a bifurcation model with a non-planar branch. *J. Biomech.* 37:1899–1911, 2004. doi:10.1016/j.jbiomech.2004.02.030.
[12]Chen, J., X. Y. Lu, and W. Wang. Non-Newtonian effects of blood flow on hemodynamics in distal vascular graft anastomoses. *J. Biomech.* 39:1983–1995, 2006. doi:10.1016/j.jbiomech.2005.06.012.
[13]Coene, P. P. L. O., A. K. Groen, P. H. P. Davids, M. Hardeman, G. N. J. Tytgat, and K. Huibregtse. Bile viscosity in patients with biliary drainage. *Scand. J. Gastroenterol.* 29:757–763, 1994. doi:10.3109/00365529409092506.
[14]Conrad, W. A. Pressure-flow relationships in collapsible tubes. *IEEE Trans. Biomech. Eng.* BME-16(4):284–295, 1969.
[15]Courtney, D. F., A. S. Clanachan, and G. W. Scott. Cholecystokinin constricts the canine cystic duct. *Gastroenterology* 85:1154–1159, 1983.
[16]Cowie, A. G. A., and D. J. Sutor. Viscosity and osmolality of abnormal bile. *Digestion* 13:312–315, 1975.
[17]Dodds, W. J., Hogan W. J., and Green, J. E. Motility of the biliary system. In: Handbook of Physiology: The Gastrointestinal System, Vol. 1, Section 6, Part 2(28), edited by S. G. Schultz. Bethesda, MD: American Physiological Society, 1989, pp. 1055–1101.
[18]Doty, J. E., H. A. Pitt, S. L. Kuchenbecker, V. Porter-Fink, and L. DenBesten. Role of gallbladder mucus in the pathogenesis of cholesterol gallstone. *Am. J. Surg.* 145:54–61, 1983. doi:10.1016/0002-9610(83)90166-6.
[19]FLUENT 6.2 Users Guide. Fluid Inc., 2005.

[20]Gijsen, F. J. H, F. N. van de Vosse, and J. D. Janssen. The influence of the non-Newtonian properties of blood on the flow in large arteries: steady flow in a carotid bifurcation model. *J. Biomech.* 32:601–608, 1999. doi:10.1016/S0021-9290(99)00015-9.

[21]Gottschalk, M., and A. Lochner. Behaviour of postoperative viscosity of bile fluid from T-drainage. *Gastroenterol. J.* 50:65–67, 1990.

[22]Hazel, A. L., and M. Heil. Steady finite-Reynolds-number flows in three-dimensional collapsible tubes. *J. Fluid Mech.* 486:79–103, 2003. doi:10.1017/S0022112003004671.

[23]Heil, M., and T. J. Pedley. Large post-buckling deformations of cylindrical shells conveying viscous flow. *J. Fluids Struct.* 10:565–599, 1996. doi:10.1006/jfls.1996.0039.

[24]Holt, J. P. Flow of liquids through collapsible tubes. *Circ. Res.* 7:342–353, 1959.

[25]Holt, J. P. Flow through collapsible tubes, through in situ veins. *IEEE Trans. Biomech. Eng.* BME-16(4):274–283, 1969.

[26]Holzbach, R. T., M. March, M. Olszewski, and K Holan. Evidence that supersaturated bile is frequent in healthy man. *J. Clin. Invest.* 52:1467–1479, 1973. doi:10.1172/JCI107321.

[27]Jungst, D., A. Niemeyer, I. Muller, B. Zundt, G. Meyer, M. Wilhelmi, and R. del Pozo. Mucin and phospholipids determine viscosity of gallbladder bile in patients with gallstones. *World J. Gastroenterol.* 7(2):203–207, 2001.

[28]Kounanis, K., and D. S. Mathoilakis. Experimental flow study within a self oscillating collapsible tube. *J. Fluids Struct.* 13:61–73, 1999. doi:10.1006/jfls.1998.0191.

[29]Li, W. G., X. Y. Luo, N. A. Hill, A. Smythe, S. B. Chin, A. G. Johnson, and N. C. Bird. Correlation of mechanical factors and gallbladder pain. *J. Comput. Math. Methods Med.* 9:27–45, 2008. doi:10.1080/17486700701780266.

[30]Li, W. G., X. Y. Luo, A. G. Johnson, N. A. Hill, N. Bird, and S. B. Chin. One-dimensional models of the human biliary system. *ASME J. Biomech. Eng.* 129:164–173, 2007. doi:10.1115/1.2472379.

[31]Luo, X. Y., W. G. Li, N. C. Bird, A. G. Johnson, S. B. Chin, and N. A. Hill. On the mechanical behaviour of human bililary system. *World J. Gastroenterol.* 13:1384–1392, 2007.

[32]Lyon, C. K., J. B. Scott, and C. Y. Wang. Flow through collapsible tubes at low Reynolds numbers. *Circ. Res.* 47(1):68–73, 1980.

[33]Marzo, A., X. Y. Luo, and C. D. Bertram. Three-dimensional collapse and steady flow in thick-walled flexible tubes. *J. Fluids Struct.* 20:817–835, 2005. doi:10.1016/j.jfluidstructs.2005.03.008.

[34]O'Callaghan, S., M. Walsh, and T. McGloughlin. Numerical modelling of Newtonian and non-Newtonian representation of blood in a distal end-to-side vascular bypass graft anastomosis. *Med. Eng. Phys.* 28:70–74, 2006. doi:10.1016/j.medengphy.2005.04.001.

[35]Ooi, R. C. Modelling flow of the bile in the human cystic duct. PhD thesis, University of Sheffield, UK, 2004.

[36]Ooi, R. C., X. Y. Luo, S. B. Chin, A. G. Johnson, and N. C. Bird. The flow of bile in the human cystic duct. *J. Biomech.* 37(13):1913–1922, 2004. doi:10.1016/j.jbiomech.2004.02.029.

[37]Pedley, T. J., B. S. Brook, and R. S. Seymour. Blood pressure and flow rate in the giraffe jugular vein. *Philos. Trans. R. Soc. Lond. B* 351:855–866, 1996. doi:10.1098/rstb.1996.0080.

[38]Pitt, H. A., J. J. Roslyn, S. L. Kuchenbecker, J. E. Doty, and L. DenBesten. The role of cystic duct resistance in the pathogenesis of cholesterol gallstones. *J. Surg. Res.* 30(5):508–514, 1981. doi:10.1016/0022-4804(81)90098-6.

[39]Portincasa, P., A. Di Ciaula, V. Palmieri, A. Velardi, G. P. Vanberge-Henegouwen, and G. Palasciano. Impaired gallbladder and gastric motility and pathological gastro-oesophageal reflux in gallstone patients. *Eur. J. Clin. Invest.* 27:653–661, 1997. doi:10.1046/j.1365-2362.1997.1600709.x.

[40]Scroggs, R. A., S. B. M. Beck, and E. A. Patterson. An integrated approach to modelling the fluid-structure interaction of a collapsible tube. *JSME Int. J. Ser. B* 47(1):20–28, 2004. doi:10.1299/jsmeb.47.20.

[41]Severi, C., J. R. Grider, and G. M. Makhlouf. Functional gradient in muscle cells isolated from gallbladder, cystic duct and common bile duct. *Am. J. Physiol.* 255:G647–G652, 1988.

[42]Tera, H. Sedimentation of bile constituents. *Ann. Surg.* 157:468–472, 1963.

[43]Thiriet, M., and C. Ribreau. Computational flow in collapsible tube with wall contact. *Mec. Ind.* 1:349–364, 2000.

[44]Thureron, E. On the stratification of human bile and its importance for the solubility of cholesterol. *Gastroenterology* 50(6):775–780, 1966.

[45]Ugural, A. C., and S. K. Fenster. Advanced Strength and Applied Elasticity. New York: Elsevier Science Publishing Co., Inc., pp. 427–428, 1987.

[46]White, F. M. Fluid Mechanics. 4th ed. New York: McGraw-Hill Book Company, pp. 342–373, 1999.

[47]Wilkinson, W. L. Non-Newtonian Fluids. London: Pergamon Press, pp. 50–52, 1960.

[48]Zhang, H., X. Zhang, S. Ji, Y. Guo, G. Ledezma, N. Elabbasi, and H. deCougny. Recent development of fluid-structure interaction capabilities in the ADINA system. *Comput. Struct.* 81:1071–1085, 2003. doi:10.1016/S0045-7949(03)00009-9.